nature astronomy

LETTERS

https://doi.org/10.1038/s41550-019-0975-9

Age dating of an early Milky Way merger via asteroseismology of the naked-eye star ν Indi

William J. Chaplin[1,2,3*], Aldo M. Serenelli[4,5], Andrea Miglio[1,2], Thierry Morel[6], J. Ted Mackereth[1,2], Fiorenzo Vincenzo[1,2,7,8], Hans Kjeldsen[2,9], Sarbani Basu[10], Warrick H. Ball[1,2], Amalie Stokholm[2], Kuldeep Verma[2], Jakob Rørsted Mosumgaard[2], Victor Silva Aguirre[2], Anwesh Mazumdar[11], Pritesh Ranadive[11], H. M. Antia[12], Yveline Lebreton[13,14], Joel Ong[10], Thierry Appourchaux[15], Timothy R. Bedding[16], Jørgen Christensen-Dalsgaard[2,3], Orlagh Creevey[17], Rafael A. García[18,19], Rasmus Handberg[2], Daniel Huber[20], Steven D. Kawaler[21], Mikkel N. Lund[2], Travis S. Metcalfe[22,23], Keivan G. Stassun[24,25], Michäel Bazot[26,27], Paul G. Beck[28,29,30], Keaton J. Bell[2,23,31], Maria Bergemann[32], Derek L. Buzasi[33], Othman Benomar[27,34], Diego Bossini[35], Lisa Bugnet[18,19], Tiago L. Campante[35,36], Zeynep Çelik Orhan[37], Enrico Corsaro[38], Lucía González-Cuesta[29,30], Guy R. Davies[1,2], Maria Pia Di Mauro[39], Ricky Egeland[40], Yvonne P. Elsworth[1,2], Patrick Gaulme[23,41], Hamed Ghasemi[42], Zhao Guo[43,44], Oliver J. Hall[1,2], Amir Hasanzadeh[45], Saskia Hekker[2,23], Rachel Howe[1,2], Jon M. Jenkins[46], Antonio Jiménez[29,30], René Kiefer[47], James S. Kuszlewicz[2,23], Thomas Kallinger[48], David W. Latham[49], Mia S. Lundkvist[2], Savita Mathur[29,30], Josefina Montalbán[1,2], Benoit Mosser[13], Andres Moya Bedón[1,2], Martin Bo Nielsen[1,2,27], Sibel Örtel[37], Ben M. Rendle[1,2], George R. Ricker[50], Thaíse S. Rodrigues[51], Ian W. Roxburgh[1,52], Hossein Safari[45], Mathew Schofield[1,2], Sara Seager[50,53,54], Barry Smalley[55], Dennis Stello[2,16,56], Róbert Szabó[57,58], Jamie Tayar[59], Nathalie Themeßl[2,23], Alexandra E. L. Thomas[1,2], Roland K. Vanderspek[50], Walter E. van Rossem[1,2], Mathieu Vrard[35,36], Achim Weiss[60], Timothy R. White[2,61], Joshua N. Winn[62] and Mutlu Yıldız[37]

Over the course of its history, the Milky Way has ingested multiple smaller satellite galaxies[1]. Although these accreted stellar populations can be forensically identified as kinematically distinct structures within the Galaxy, it is difficult in general to date precisely the age at which any one merger occurred. Recent results have revealed a population of stars that were accreted via the collision of a dwarf galaxy, called Gaia–Enceladus[1], leading to substantial pollution of the chemical and dynamical properties of the Milky Way. Here we identify the very bright, naked-eye star ν Indi as an indicator of the age of the early in situ population of the Galaxy. We combine asteroseismic, spectroscopic, astrometric and kinematic observations to show that this metal-poor, alpha-element-rich star was an indigenous member of the halo, and we measure its age to be 11.0 ± 0.7 (stat) ±0.8 (sys) billion years. The star bears hallmarks consistent with having been kinematically heated by the Gaia–Enceladus collision. Its age implies that the earliest the merger could have begun was 11.6 and 13.2 billion years ago, at 68% and 95% confidence, respectively. Computations based on hierarchical cosmological models slightly reduce the above limits.

The recently launched NASA Transiting Exoplanet Survey Satellite (TESS)[2] has opened up the brightest stars across about 80% of the sky[3] to micro-magnitude photometric studies in its two-year nominal mission. These are stars visible to the naked eye, which present huge opportunities for detailed characterization, study and follow-up. ν Indi (HR 8515; HD 211998; HIP 110618) is a very bright (visual apparent magnitude $V = 5.3$) metal-poor subgiant, which was observed by TESS during its first month of science operations. Using nearly continuous photometric data with two-minute time sampling, we are able to measure a rich spectrum of solar-like oscillations in the star. By combining these asteroseismic data with re-analysed chemical abundances from ground-based spectroscopy, together with astrometry and kinematics from the Gaia Data Release 2 (DR2)[4], we show this single star to be a powerful, representative tracer of old, in situ stellar populations in the Galaxy. The results on ν Indi allow us to place fresh constraints on the age of the in situ halo and the epoch of the Gaia–Enceladus merger.

We re-analysed archival high-resolution spectroscopic data on ν Indi collected by the High Accuracy Radial velocity Planet Searcher (HARPS) spectrograph[5] on the European Southern Observatory (ESO) 3.6-m telescope at La Silla, Chile, and by the Fiber-fed Extended Range Optical Spectrograph (FEROS)[6] on the 2.2-m ESO/MPG telescope (also at La Silla). From these high-resolution spectra we measured the overall iron abundance and detailed abundances for 20 different elements, providing a comprehensive set of data on

A full list of affiliations appears at the end of the paper.

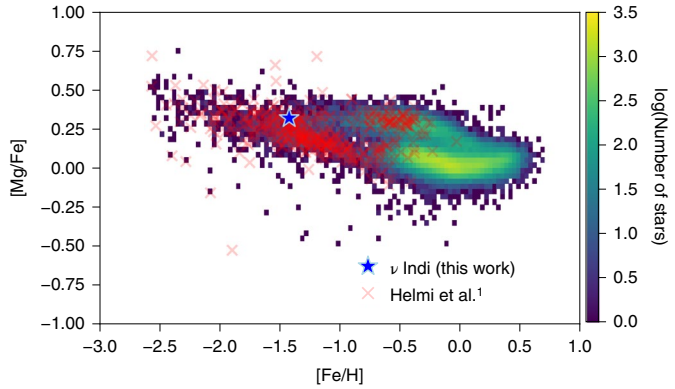

Fig. 1 | [Mg/Fe] versus [Fe/H] abundances of a large sample of Milky Way stars, from the APOGEE DR-14 spectroscopic survey data release[8]. Results for ν Indi are marked by the blue star-shaped symbol. Points in red show the sample of stars identified as being part of the accreted population from Gaia–Enceladus[1].

the chemistry of the star (see Methods for table of abundances and further details). ν Indi exhibits enhanced levels of alpha-process elements in its spectrum, that is, elements heavier than carbon produced by nuclear reactions involving helium. The logarithmic abundance relative to iron is $[\alpha/\mathrm{Fe}] = +0.4$. Among Galactic disk stars, elevated $[\alpha/\mathrm{Fe}]$ levels are associated with old stellar populations. ν Indi shows an overabundance of titanium of $[\mathrm{Ti/Fe}] = +0.27 \pm 0.07$, which puts it in the regime where a previous study[7] found ages exceeding about 9.5 billion years (Gyr) for alpha-enhanced stars in the local solar neighbourhood, where ν Indi resides.

Figure 1 shows [Mg/Fe] abundances of Milky Way stars, including ν Indi, from the Apache Point Observatory Galaxy Evolution Experiment (APOGEE) DR-14 spectroscopic survey release[8] (see Methods for further details). ν Indi's abundances place it at the upper edge of the distribution identified with the accreted Gaia–Enceladus population[1] (points in red at lower [Mg/Fe]); but more in line with the in situ halo population at higher [Mg/Fe]. Were it to have been accreted, it is unlikely the star could be a member of a different accreted population, because its high [Mg/Fe] would suggest the progenitor dwarf galaxy would have had to have been at least as massive as Gaia–Enceladus. Since the stellar debris from Gaia–Enceladus is thought to make up a high fraction of the stellar mass of the present-day halo, it seems improbable that there could exist another similar undiscovered satellite. We therefore conclude, on the basis of chemistry alone, that ν Indi is either a member of the in situ population, or a member of Gaia–Enceladus. We now use kinematics to show that the former is most likely to be correct.

To place ν Indi in context among other stars with similar elemental abundances, we selected stars from APOGEE-DR14 having [Fe/H] equal (within the uncertainties) to our measured value for ν Indi. Figure 2 shows Gaia-DR2 velocity data for populations with low and high [Mg/Fe], which divides the stars roughly equally into accreted and in situ halo stars[9,10]. The cross-hair marks the location of ν Indi on both plots. The low-[Mg/Fe] group includes many stars in the high-eccentricity accreted halo, which was recently determined to be dominated by the Gaia–Enceladus accretion event. Here, the low-[Mg/Fe] population shows a flat distribution (the so-called Gaia Sausage) in the tangential velocity versus radial velocity plane, consistent with the strong radial motion from an accreted population. In the vertical velocity versus radial velocity plane, the distributions of the low- and high-[Mg/Fe] stars are remarkably similar. This suggests that the in situ, higher-[Mg/Fe] population, which includes ν Indi (see below), was heated by the accreted

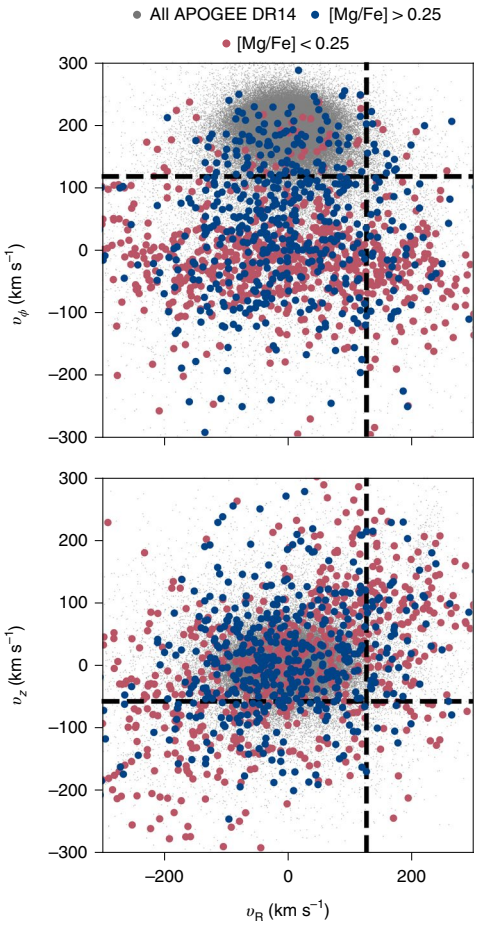

Fig. 2 | Velocities of stars from APOGEE-DR14 having [Fe/H] values within uncertainties of the [Fe/H] value of ν Indi. The points in blue show results for 637 stars with [Mg/Fe]> + 0.25, while those in red are for 918 stars with [Mg/Fe] < + 0.25. Results for the full APOGEE-DR14 sample are plotted in grey. Tangential velocity (upper panel) and vertical velocity (lower panel) are plotted, in Galacto-centric cylindrical coordinates and as a function of radial velocity. The dashed cross-hair marks the location of ν Indi in these planes.

population. We note also evidence from simulations[11–13] for mergers causing heating of in situ populations.

We derived Galactic orbital parameters for ν Indi using the positions and velocities provided by Gaia-DR2 (see Methods). We performed the same orbital integrations for the populations with low and high [Mg/Fe]. Figure 3 shows a contour plot of the resulting distributions of the eccentricity, e, and maximum vertical excursion from the Galactic mid-plane, z_{max}. Low-eccentricity orbits are dominated by higher-[Mg/Fe] stars, and are probably part of the thick disk/in situ halo. The position of ν Indi is marked on the contour plot as a circle; the uncertainties are too small to be visible on this scale. Our analysis of the Gaia-DR2 data reveals that ν Indi has a relatively eccentric orbit, with $e = 0.60 \pm 0.01$, $z_{\mathrm{max}} = 1.51 \pm 0.02$ kpc, and a Galactic pericentric radius of $\simeq$2.5 kpc. Given that ν Indi lies in a region of kinematics space dominated by the higher-[Mg/Fe] stars, and has an [Mg/Fe] abundance corresponding to that of those stars, it is likely to be a member of this population, formed in situ (five times more likely than not, based on the data in Figs. 2 and 3).

From the discussion above we find that ν Indi is an in situ star whose age can provide insights on the origin of the low-[Fe/H], high-[Mg/Fe] population to which it belongs. The new asteroseismic data from TESS provide the means of constraining the age very

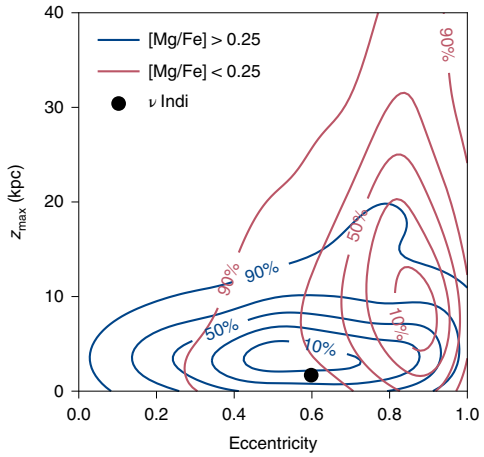

Fig. 3 | Contour plot of the distribution in eccentricity, *e*, and maximum vertical excursion from the Galactic mid-plane, z_{max}, for the same high-[Mg/Fe] (blue) and low-[Mg/Fe] (red) samples of stars as Fig. 2. The solid black circle marks the location of ν Indi. The contours are marked with the corresponding cumulative probabilities for each sample.

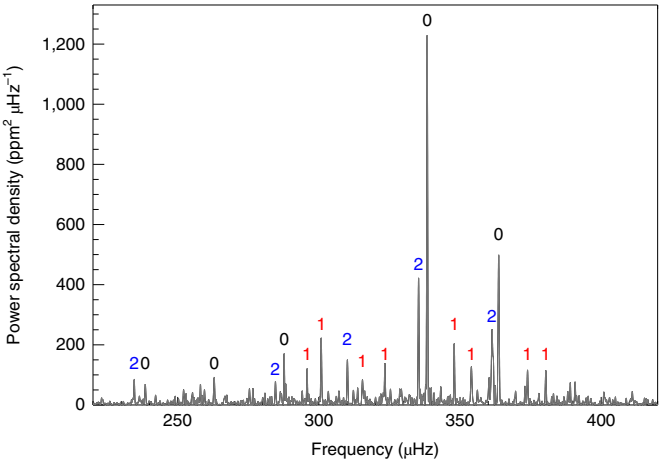

Fig. 4 | Frequency–power spectrum of the TESS lightcurve of ν Indi, showing a rich spectrum of solar-like oscillations. The ordinate is in power spectral density (PSD) units of parts per million squared per μHz. Marked on the plot are the angular degrees, *l*, of modes whose frequencies we reported in order to model the star.

precisely. ν Indi was included on the two-minute cadence list by the TESS Asteroseismic Science Consortium (TASC) as a prime target for asteroseismology[14]. It was observed for just over 27 days in sector 1 of the TESS science operations. Figure 4 shows the frequency–power spectrum of the calibrated lightcurve (see Methods).

The star shows a rich spectrum of overtones of solar-like oscillations, modes that are stochastically excited and intrinsically damped by near-surface convection[15]. The modes may be decomposed onto spherical harmonics of angular degree *l*. Overtones of radial ($l=0$), dipole ($l=1$) and quadrupole ($l=2$) modes are clearly seen. Because ν Indi is an evolved star, its non-radial modes are not pure acoustic modes. They show so-called 'mixed' character[16], caused by coupling with waves confined in cavities deep within the star for which buoyancy, as opposed to gradients of pressure, acts as the restoring force. Frequencies of mixed modes change rapidly with time as the star evolves towards the red-giant phase, and are very sensitive to the structure of the deepest-lying layers, thus providing strong diagnostic constraints on the age and structure of a star. Previous ground-based observations of precise Doppler shifts had detected solar-like oscillations in ν Indi[17], but with just a few days of data only a few oscillation modes could be identified[18]. With TESS, there is no ambiguity across several orders of the spectrum, and we measured precise frequencies of 18 modes spanning six overtones (see Table 1 and Methods for further details).

To constrain the mass and age of ν Indi we used as input the measured oscillation frequencies; the spectroscopically estimated effective temperature, [Fe/H] abundance and the [α/Fe] ratio; and, as another observational constraint, the stellar luminosity given by the Gaia-DR2 parallax and the Tycho 2[19] V- and B-band magnitudes. These inputs were compared, using well developed modelling techniques[20], to intrinsic properties and predicted observables of stellar evolutionary models in evolutionary sequences sampling a grid dense in mass and composition. We find a mass of 0.85 ± 0.04 (stat) ±0.02 (sys) $M_{\odot}$ and an age of 11.0 ± 0.7 (stat) ±0.8 (sys) Gyr. The precision achieved in mass and age is notably inferior when the asteroseismic inputs are not used.

The asteroseismic age is consistent with the claim that stars in the region of [Mg/Fe]–[Fe/H] space that includes ν Indi were heated kinematically by the Gaia–Enceladus merger. That episode has been estimated to have occurred between 9 and 12 Gyr ago[1,21,22]. Recent results also indicate that the in situ halo was in place prior to the merger[22]. We may therefore use the age of ν Indi to place a new limit on the earliest epoch at which the merger occurred (that is, the star must have already been in place). We must take into account the uncertainty on our estimated age, and the potential duration in time of the merger itself. Numerical simulations in the literature suggest timescales for the relevant mass range of between 1 and 2 Gyr (ref. [23]). Using our posterior on the age of ν Indi, and allowing for a spread of up to 2 Gyr for the merger, we estimate that the earliest the merger could have begun was 11.6 Gyr ago at 68% confidence and 13.2 Gyr ago at 95% confidence (see Methods and Extended Data Figs. 2 and 3). The results are fairly insensitive to the merger duration (for example, reducing the duration to 1 Gyr reduces the 95% limit by 0.3 Gyr). Theoretical computations, based on hierarchical

Table 1 | Measured oscillation frequencies of ν Indi, with 1σ uncertainties

Degree, *l*	Frequency (μHz)	Uncertainty (μHz)
2	234.60	0.18
0	238.52	0.20
0	262.93	0.18
2	284.62	0.18
0	287.72	0.13
1	295.81	0.14
1	300.84	0.11
2	310.10	0.13
1	315.44	0.19
1	323.41	0.15
2	335.33	0.07
0	338.38	0.05
1	347.96	0.11
1	353.98	0.15
2	361.33	0.11
0	363.70	0.07
1	373.91	0.15
1	380.39	0.17

Table 2 | Spectroscopically derived abundances

Element	Unconstrained abundance	Constrained abundance
[Fe/H]*	–1.46±0.07 (58,5)	–1.43±0.06 (58,5)
[Li/H]	–0.01±0.09 (1)	+0.04±0.07 (1)
[C/Fe]	+0.33±0.09 (1)	+0.31±0.08 (1)
[O/Fe] (O I)*	+0.60±0.10 (2)	+0.56±0.09 (2)
[O/Fe] ([O I])*	+0.41±0.09 (1)	+0.45±0.08 (1)
[Na/Fe]	–0.20±0.10 (2)	–0.21±0.10 (2)
[Mg/Fe]*	+0.34±0.08 (1)	+0.32±0.08 (1)
[Si/Fe]*	+0.18±0.06 (7)	+0.17±0.06 (7)
[Ca/Fe]*	+0.41±0.07 (6)	+0.40±0.06 (6)
[Sc/Fe]	+0.00±0.06 (2)	+0.02±0.06 (2)
[Ti/Fe]	+0.27±0.07 (4)	+0.27±0.07 (4)
[V/Fe]	+0.00±0.12 (3)	+0.02±0.11 (3)
[Cr/Fe]*	–0.13±0.08 (1)	–0.14±0.08 (1)
[Mn/Fe]*	–0.23±0.08 (3)	–0.23±0.07 (3)
[Co/Fe]	+0.18±0.10 (3)	+0.19±0.09 (3)
[Ni/Fe]	–0.08±0.07 (13)	–0.08±0.07 (13)
[Cu/Fe]	–0.38±0.08 (1)	–0.39±0.08 (1)
[Zn/Fe]	+0.16±0.09 (1)	+0.15±0.09 (1)
[Y/Fe]	+0.08±0.07 (3)	+0.10±0.07 (3)
[Zr/Fe]	+0.38±0.08 (1)	+0.40±0.08 (1)
[Ba/Fe]	–0.02±0.13 (2)	+0.00±0.13 (2)

Values in brackets give the number of features each abundance is based on. For iron, the number of Fe I and Fe II lines is given. The final iron abundance is the unweighted average of the Fe I- and Fe II-based values. Abundances corrected for NLTE effects are marked by an asterisk. Error ranges represent 1σ uncertainties.

cosmological models (again, see Methods), suggest a low probability that the merger occurred before ν Indi formed. Including this information tightens (that is, reduces) slightly the above limits.

Methods

Spectroscopic analysis. The results of our detailed spectroscopic analysis are presented in Table 2. It shows spectroscopically derived abundances and 1σ uncertainties, without (unconstrained) and with (constrained) an asteroseismic constraint on logg.

We base the analysis primarily on the average of six HARPS spectra obtained in December 2007, retrieved from the instrument archives. They have a resolving power R of 115,000 and cover the spectral domain from 379 nm to 691 nm (with a gap between 530.4 nm and 533.8 m). The signal-to-noise ratio at 550 nm lies in the range 177 to 281. We carried out a differential, line-by-line analysis relative to the Sun. The high-quality (signal-to-noise ratio approximately 470) solar HARPS spectrum was taken from the online library of Gaia FGK benchmarks[24]. It is a solar reflected spectrum from asteroids with a similar resolution to that of the spectra for ν Indi. For oxygen we made use of the OI triplet at about 777.4 nm. Because this range is not covered by the HARPS spectra, we used the spectrum available in the FEROS archives (R about 47,000 and a mean signal-to-noise ratio of 340). For the Sun, numerous asteroid spectra were considered. All the spectra were normalized to the continuum by fitting low-order cubic spline or Legendre polynomials to the line-free regions using standard tasks implemented in the IRAF software[25].

The stellar parameters and abundances of 20 elements were determined self-consistently from the spectra, plane-parallel MARCS model atmospheres[26], and the 2017 version of the line-analysis software MOOG. We used a line list[27] augmented[28,29] for C I, Sc II, Mn I, Co I, Cu I, Zn I, Y II and Zr II. Equivalent widths (EWs) were measured manually, assuming Gaussian profiles. Only lines above 480.0 nm were considered because of strong line crowding in the blue that leads to an uncertain placement of the continuum. With the exception of Mg I at wavelength $\lambda = 571.1$, lines with relative width RW = log(EW/λ) > 4.8 were discarded. Hyperfine structure and isotopic splitting were taken into account for Sc, V, Mn, Co and Cu using atomic data from the Kurucz database with an assumed Cu isotopic ratio[30]. The `blends` driver in MOOG was employed for the analysis. The corrections are very small for ν Indi, but can be substantial for the Sun. The determination of the Li and O abundances from Li I λ = 670.8 and [O I] λ = 630.0 relied on a spectral synthesis[31], taking the macroturbulent and projected rotational velocities of ν Indi into account[32].

The four model parameters—effective temperature $T_{\rm eff}$, surface gravity logg, metallicity [Fe/H] and microturbulence parameter ξ—were modified iteratively until the excitation and ionization balance of iron was fulfilled and the Fe I abundances exhibited no trend with RW. The abundances of iron and the alpha elements were also required to be consistent with the values adopted for the model atmosphere. For the solar analysis, $T_{\rm eff}$ and logg were held fixed at 5,777 K and 4.44 dex, respectively, whereas the microturbulence ξ was left as a free parameter (we obtained $\xi_{\odot} = 0.97$ km s^{-1}). We also performed the analysis with the surface gravity of ν Indi fixed to the asteroseismic value of logg = 3.46 dex in order to increase both the accuracy and precision of the spectroscopic results. For this constrained analysis, we adjusted $T_{\rm eff}$ to satisfy the iron ionization equilibrium.

The uncertainties in the stellar parameters and abundances were computed following well established procedures[33]. In particular, the analysis was repeated using Kurucz atmosphere models and the differences incorporated in the error budget. However, the deviations with respect to the default values (Kurucz minus MARCS) appear to be small: $\Delta T_{\rm eff} = -15$ K, Δlogg = −0.01, and abundance ratios deviating by less than 0.01 dex.

We also computed corrections to the abundances for non-local-thermodynamic-equilibrium (NLTE) effects, with those corrections defined as the difference in abundance required to fit a line profile using either NLTE or local-thermodynamic-equilibrium (LTE) models. The NLTE corrections were estimated for most of the spectral lines in the LTE analysis using the interactive online tool at `nlte.mpia.de`. Corrections for ν Indi were computed using a MARCS model atmosphere. We also computed corrections for the Sun, but using a more appropriate MAFAGS-OS model, and subtracted the solar corrections from the corrections for ν Indi in order to compensate for the LTE minus NLTE differences in the reference regime. We note that the difference between MARCS and MAFAGS is negligible for main-sequence stars[34].

We used the online tool to compute corrections for O, Mg, Si, Ca and Cr. The data used are based on the NLTE model *atoms*[34–38]. NLTE corrections for the lines of Mn were computed separately[39,40], as these atoms are not yet a part of the publicly released grid that is coupled to the online tool. For several elements, no NLTE data are available in the literature.

We found corrections that are typically within the quoted abundance uncertainties—for example, the correction to the overall Iron abundance [Fe/H] was 0.07—which do not have a substantial impact on the estimated fundamental properties of the star.

The above analyses yielded an estimated effective temperature of $T_{\rm eff} = 5,320 \pm 24$ K from the asteroseismically constrained analysis and $T_{\rm eff} = 5,275 \pm 45$ K from the unconstrained analysis; and a NLTE-corrected metallicity of [Fe/H] = −1.43 ± 0.06 from the constrained analysis, and [Fe/H] = −1.46 ± 0.07 from the unconstrained analysis. Detailed chemical abundances are listed in Table 2. The values in brackets give the number of features each abundance is based on. For iron, the number of Fe I and Fe II lines is given. The final iron abundance is the unweighted average of the Fe I and Fe II values. For oxygen, we adopt the value given by [O I] λ 630 because it is largely insensitive to non-LTE and three-dimensional effects. We also analysed the chromospheric activity of ν Indi using 116 archival Ca HK spectra from the SMARTS Southern HK programme, obtained 2007–2012. The median S-index calibrated to the Mount Wilson scale is 0.138, which is converted to the bolometric-relative HK flux $\log(R^{'}_{\rm HK}) = -5.16$ using an empirical relation[41] and the colour index $B - V = 0.65$. This is in good agreement with other results in the literature[42]. Chromospheric activity is a well known proxy for age, and this low value is consistent with a very old star[43]. The empirical age–activity relationship[44] is calibrated to a low activity limit of $\log(R^{'}_{\rm HK}) = -5.10$, corresponding to a lower-limit age of 8.4 Gyr with an estimated uncertainty of 60%, consistent with the result from our asteroseismic analysis.

APOGEE-DR14 and Gaia-DR2 analysis. To construct Fig. 1 of the main paper, we used abundances from the Fourteenth Data Release (DR-14) of the SDSS IV-APOGEE survey, which obtained high resolution ($R \simeq 20,000$), high signal-to-noise ratio (SNR ≃ 100 per pixel) spectra in the near-infrared H-band. We take the calibrated [Fe/H] and [Mg/Fe] abundances directly from the APOGEE DR-14 catalogue, selecting only stars that form part of the main survey (that is, part of the 'statistical sample'). We also performed a cross-match between this catalogue and the stars identified[1] as being part of the Gaia–Enceladus population on the basis of their angular momenta (as measured using Gaia-DR2 data); as such, this population is likely to be contaminated by thick-disk stars, which have considerably higher [Fe/H] and [Mg/Fe] than the true Gaia–Enceladus populations.

For the kinematics analysis (Figs. 2 and 3), we used the six-dimensional information (positions and velocities) provided by Gaia-DR2 to derive Galactic orbital parameters for ν Indi, as well as stars from APOGEE-DR14 having [Fe/H] equal (within the uncertainties) to our measured value for ν Indi. APOGEE stars were targeted[45,46] based on their $(J - K)$ colour and H-band magnitude alone, and so the selection does not result in any substantial kinematic biases to the data. More than 90% of the APOGEE stars we selected have a Gaia-DR2 proper motion.

By reconstructing and taking samples from the covariance matrix of the astrometric parameters, we performed orbital integrations from 1,000 realizations of the initial phase-space coordinates of the star. We used the Python package `galpy`[47], adopting a Milky-Way-like potential (having verified that reasonable changes to the potential did not affect the conclusions drawn from our results). To convert between the observed astrometric parameters (positions, parallaxes, proper motions and radial velocities) and Galactocentric positions and velocities we adopted the Galactocentric distance of the GRAVITY collaboration[48] of 8.127 kpc, the height $z_0 = 0.02$ kpc of the Sun above the midplane of the Galaxy[49], and a solar velocity from a recent re-assessment of the stellar kinematics of the solar neighbourhood[50].

Asteroseismic analysis. The TESS target pixel file data for ν Indi were produced by the TESS Science Operations Center (SPOC)[51], and are available at the Mikulski Archive for Space Telescopes (MAST) (http://archive.stsci.edu/). The lightcurve we analysed was extracted from target pixel files by the TESS Asteroseismic Science Operations Centre (TASOC) pipeline[52]. A rich spectrum of overtones of radial- and non-radial solar-like oscillations is clearly detectable (see Fig. 4). Even though the modes are intrinsically damped, the lifetimes are longer than the 27-day length of the TESS data. The modes may as such be treated as being coherent on the timescale of the lightcurve, and we extracted their frequencies using a well tested weighted sine-wave fitting analysis[53,54], which allowed for the varying quality of the TESS photometry over the period of observation. Approaches based on fitting Lorentzian-like models to the resonant peaks[55–65] gave very similar results. Corrections to the frequencies to allow for the line-of-sight velocity of the star[66] are very small, and do not change the inferred stellar properties. The list of frequencies, together with equivalent 1 σ uncertainties, is presented in Table 1.

The oscillation frequencies were used as input to the stellar modelling, along with spectroscopically derived effective temperature $T_{\rm eff}$, metallicity [Fe/H], and α-enhancement, [α/Fe], all from the asteroseismically constrained analysis, and an estimate of the stellar luminosity $L = 6.00 \pm 0.35\ L_{\odot}$, using the Gaia-DR2 parallax and the Tycho 2 V- and B-band magnitudes[19], and a bolometric correction appropriate to the alpha-enhanced composition[67] (and assuming negligible extinction). We note that a spectral energy distribution (SED) fit[68] gave similar constraints on luminosity.

Prior to use in the modelling we inflated the uncertainties on $T_{\rm eff}$ and [Fe/H] to account for systematic differences between spectroscopic methods by adding, respectively, 59 K and 0.062 in quadrature to the formal uncertainties[69], yielding final values of $T_{\rm eff} = 5,320 \pm 64$ K and [Fe/H]$= -1.43 \pm 0.09$.

ν Indi is a metal-poor star showing noticeable alpha enhancement, which affects the mapping of [Fe/H] to the metal-to-hydrogen abundance ratio Z/X. Some modellers used grids of stellar evolutionary models that did not include the requisite enrichment, and under such circumstances a correction must be applied to the raw [Fe/H] to allow it to be used in modelling using those grids. Here, the correction needed[70] is +0.25. This gave a corrected metallicity of [Fe/H]$= -1.18 \pm 0.11$, where the error bar was inflated further to account for uncertainty in the correction.

Various codes[20,71–77] were used to model the star and to explore its fundamental stellar properties. ν Indi is in a rapid stage of stellar evolution, and we found it was imperative that the codes interrogated model grids sampled at a fine resolution in mass and metallicity in order to obtain a good match of predicted observables of the best-fitting model to the actual observables. Our best-fitting estimates are 0.85 ± 0.04 (stat) ± 0.02 (sys) $M_{\odot}$ and an age of 11.0 ± 0.7 (stat) ± 0.8 (sys) Gyr. The central values and statistical uncertainties were provided by one of the codes[20], which returned the best match to the input data. The systematic uncertainties reflect the scatter between different results. In all cases, the errors correspond to a 68% confidence level.

Extended Data Fig. 1 is an échelle diagram showing the match between the observed frequencies (in grey) and the best-fitting model frequencies (coloured symbols).

We also tested the impact of removing the asteroseismic frequencies from the modelling. This inflated the fractional uncertainty on the mass (statistical uncertainty) from ≃5% to ≃8%, and the fractional uncertainty on age from less than 10% to more than 30%.

Gaia–Enceladus epoch analysis. Our estimated age for ν Indi was used to place a new limit on the earliest epoch at which the Gaia–Enceladus merger occurred. This took into account the uncertainty on the estimated age, and the potential duration in time of the merger itself. Extended Data Figs. 2 and 3 capture these results, as we explain below.

To place constraints on the duration of the merger, we estimated the dynamical friction timescale for the orbit of Gaia-Enceladus to decay due to the drag force exerted on it by the diffuse dark-matter halo of the Milky Way. We adopted a widely used formulation[78], assumed that at the epoch of the merger the mass ratio between Gaia–Enceladus and our Galaxy was one-quarter[1], and that the orbit of Gaia–Enceladus was strongly radialized[79]. This procedure gave a merger timescale of less than or around 1 Gyr. Numerical simulations in the literature suggest timescales for the relevant mass range that are between 1 and 2 Gyr (ref. [23]). Here, we adopt the largest value of 2 Gyr.

To estimate the limit on the epoch of the merger we started from the probability distribution on the age of ν Indi but considered the cumulative probability distribution function, which expresses the probability of the existence of the star at any given epoch (plotted as a dashed line in Extended Data Figs. 2 and 3). The probability tends to unity at epochs more recent than the central age estimate, and to zero at epochs earlier than the central age estimate. (Note that we combined the statistical and systematic errors in quadrature, so that the distribution is described by a mean of 11 Gyr and a standard deviation of 1.1 Gyr.) If the merger was instantaneous, the above distribution function would give us the sought-for limit on the earliest possible epoch. But it is not, and so we used a Gaussian distribution to describe the merger, having a full-width at half-maximum (FWHM) of up to 2 Gyr. We may consider this function as describing the probability of interaction of the merger with ν Indi. When convolved with the cumulative age probability distribution of the star, we obtain the cumulative probability for the merger (solid black line in Extended Data Figs. 2 and 3), and limits on the earliest epoch of merger of 11.6 Gyr ago at 68% confidence, and 13.2 Gyr ago at 95% confidence.

We then folded in a theoretical prior on the probability of occurrence of the merger at different epochs, based on hierarchical cosmological models of structure formation. We estimated a cumulative prior probability using the Press–Schechter formalism[78,80], as the conditional cumulative probability $\mathcal{P}(t < t_{\rm merg}) = \mathcal{P}(M_{\rm MW}, t < t_{\rm merg} | M_{\rm Enc}, t_{\rm Enc})$ that the Enceladus dark matter halo (of mass $M_{\rm Enc}$) formed at time $t_{\rm Enc}$ and was later incorporated into the larger Milky Way dark-matter halo (of mass $M_{\rm MW}$) already in place at the time of the merger $t = t_{\rm merg}$, which is the independent variable in our computation. We assumed values for the virial mass of the *Gaia*-Enceladus dark matter halo between a lower limit of $M_{\rm Enc} = 1 \times 10^{10}$ $M_{\odot}$[79] and 1×10^{11} $M_{\odot}$[79,81], formed at the cosmic time $t_{\rm Enc} = 1.5$ Gyr which corresponds to the observed median age of *Gaia*-Enceladus stars[22]. Finally we assumed that at the epoch of merger the Milky Way dark matter halo had a Virial mass $M_{\rm MW} = 4 \times 10^{11}$ $M_{\odot}$, which has been derived at redshift $z = 2$ from the predicted cosmological halo mass accretion history of a Milky-Way-like galaxy[82–84].

Priors are plotted as a dot-dashed line for $M_{\rm Enc} = 1 \times 10^{10}$ $M_{\odot}$ in Extended Data Fig. 2, and 1×10^{11} $M_{\odot}$ in Extended Data Fig. 3. Both suggest there was a low probability of the merger occurring prior to the formation of ν Indi. Including the prior, we obtain the cumulative probabilities for the merger shown by the red lines in both figures, which tighten the limiting epoch (at 95% confidence) to 11.7 Gyr for $M_{\rm Enc} = 1 \times 10^{10}$ $M_{\odot}$ (Extended Data Fig. 2), and 12.4 Gyr for $M_{\rm Enc} = 1 \times 10^{11}$ $M_{\odot}$ (Extended Data Fig. 3). We also tested the impact of varying $t_{\rm Enc}$ by a ± 1 Gyr, and using a Milky Way mass up to 10^{12} $M_{\odot}$. These variations gave changes of up to ≃0.5 Gyr in the inferred limit on the merger epoch; but overall the tendency is to tighten the limit obtained without the prior.

Data availability

Raw TESS data are available from the MAST portal at https://archive.stsci.edu/access-mast-data. The TASOC lightcurve is available at https://tasoc.dk/. The TESS lightcurve and power spectrum is also available on request from the corresponding author. The high-resolution spectroscopic data are available at http://archive.eso.org/wdb/wdb/adp/phase3_spectral/form (HARPS ν Indi), https://www.blancocuaresma.com/s/benchmarkstars (HARPS solar spectrum), and http://archive.eso.org/wdb/wdb/adp/phase3_spectral/form (FEROS). MARCS model atmospheres are available at http://marcs.astro.uu.se/. APOGEE Data Release 14 may be accessed via https://www.sdss.org/dr14/.

Code availability

The adopted asteroseismic modelling results were provided by the BeSPP code, which is available on request from A.M.S. (aldos@ice.csic.es). NLTE corrections were estimated using the interactive online tool at http://nlte.mpia.de. The computation of Kurucz models with ATLAS9 was performed using http://atmos.obspm.fr/index.php/documentation/7. Publicly available codes used to model the data include IRAF (http://ast.noao.edu/data/software), MOOG (https://www.as.utexas.edu/chris/moog.html), the MCMC code `emcee` (https://github.com/dfm/emcee), the peak-bagging codes DIAMONDS (https://github.com/EnricoCorsaro/DIAMONDS) and TAMCMC-C (https://github.com/OthmanB/TAMCMC-C), the stellar evolution code MESA (http://mesa.sourceforge.net/), and the stellar pulsation code GYRE (https://bitbucket.org/rhdtownsend/gyre/wiki/Home). Other codes used in the analysis—including frequency analysis tools—are available on reasonable request via the corresponding author.

Received: 14 October 2019; Accepted: 13 November 2019;
Published online: 13 January 2020

References

1. Helmi, A. et al. The merger that led to the formation of the Milky Way as inner stellar halo and thick disk. *Nature* **563**, 85–88 (2018).
2. Ricker, G. R. et al. Transiting Exoplanet Survey Satellite (TESS). In *Space Telescopes and Instrumentation 2014: Optical, Infrared, and Millimeter Wave* Vol. 9143 *Proc. SPIE* 914320 (2014).

3. Stassun, K. G. et al. The TESS input catalog and candidate target list. *Astron. J.* **156**, 102 (2018).
4. GaiaCollaboration et al. Gaia Data Release 2. Summary of the contents and survey properties. *Astron. Astrophys.* **616**, A1 (2018).
5. Mayor, M. et al. Setting new standards with HARPS. *Messenger* **114**, 20–24 (2003).
6. Kaufer, A. et al. Commissioning FEROS, the new high-resolution spectrograph at La Silla. *Messenger* **95**, 8–12 (1999).
7. Bensby, T., Feltzing, S. & Oey, M. S. Exploring the Milky Way stellar disk. A detailed elemental abundance study of 714 F and G dwarf stars in the solar neighbourhood. *Astron. Astrophys.* **562**, A71 (2014).
8. Majewski, S. R. et al. The Apache Point Observatory Galactic Evolution Experiment (APOGEE). *Astron. J.* **154**, 94 (2017).
9. Hayes, C. R. et al. Disentangling the Galactic halo with APOGEE. I. Chemical and kinematical investigation of distinct metal-poor populations. *Astrophys. J.* **852**, 49 (2018).
10. Mackereth, J. T. et al. The origin of accreted stellar halo populations in the Milky Way using APOGEE, Gaia, and the EAGLE simulations. *Mon. Not. R. Astron. Soc.* **482**, 3426–3442 (2019).
11. Font, A. S. et al. Cosmological simulations of the formation of the stellar haloes around disc galaxies. *Mon. Not. R. Astron. Soc.* **416**, 2802–2820 (2011).
12. McCarthy, I. G. et al. Global structure and kinematics of stellar haloes in cosmological hydrodynamic simulations. *Mon. Not. R. Astron. Soc.* **420**, 2245–2262 (2012).
13. Tissera, P. B. et al. The central spheroids of Milky Way mass-sized galaxies. *Mon. Not. R. Astron. Soc.* **473**, 1656–1666 (2018).
14. Schofield, M. et al. The asteroseismic target list for solar-like oscillators observed in 2 minute cadence with the transiting exoplanet survey satellite. *Astrophys. J. Suppl. Ser.* **241**, 12 (2019).
15. Chaplin, W. J. & Miglio, A. Asteroseismology of solar-type and red-giant stars. *Annu. Rev. Astron. Astrophys.* **51**, 353–392 (2013).
16. Bedding, T. R. et al. Gravity modes as a way to distinguish between hydrogen- and helium-burning red giant stars. *Nature* **471**, 608–611 (2011).
17. Bedding, T. R. et al. Solar-like oscillations in the metal-poor subgiant *V* Indi: constraining the mass and age using asteroseismology. *Astrophys. J.* **647**, 558–563 (2006).
18. Carrier, F. et al. Solar-like oscillations in the metal-poor subgiant ν Indi. II. Acoustic spectrum and mode lifetime. *Astron. Astrophys.* **470**, 1059–1063 (2007).
19. Høg, E. et al. The Tycho-2 catalogue of the 2.5 million brightest stars. *Astron. Astrophys.* **355**, L27–L30 (2000).
20. Serenelli, A. et al. The first APOKASC catalog of Kepler dwarf and subgiant stars. *Astrophys. J. Suppl. Ser.* **233**, 23 (2017).
21. Vincenzo, F. et al. The fall of a giant. Chemical evolution of Enceladus, alias the Gaia sausage. *Mon. Not. R. Astron. Soc.* **487**, L47–L52 (2019).
22. Gallart, C. et al. Uncovering the birth of the Milky Way through accurate stellar ages with Gaia. *Nat. Astron.* **3**, 932–939 (2019).
23. Velazquez, H. & White, S. D. M. Sinking satellites and the heating of galaxy discs. *Mon. Not. R. Astron. Soc.* **304**, 254–270 (1999).
24. Blanco-Cuaresma, S., Soubiran, C., Jofré, P. & Heiter, U. The Gaia FGK benchmark stars. High resolution spectral library. *Astron. Astrophys.* **566**, A98 (2014).
25. Tody, D. The IRAF Data Reduction and Analysis System. In *Instrumentation in Astronomy VI* (ed. Crawford, D. L.) Vol. 627 *SPIE Conf. Ser.* 733 (1986).
26. Gustafsson, B. et al. A grid of MARCS model atmospheres for late-type stars. I. Methods and general properties. *Astron. Astrophys.* **486**, 951–970 (2008).
27. Chen, Y. Q., Nissen, P. E., Zhao, G., Zhang, H. W. & Benoni, T. Chemical composition of 90 F and G disk dwarfs. *Astron. Astrophys. Suppl.* **141**, 491–506 (2000).
28. Meléndez, J. et al. 18 Sco: a solar twin rich in refractory and neutron-capture elements. Implications for chemical tagging. *Astrophys. J.* **791**, 14 (2014).
29. Reddy, B. E., Tomkin, J., Lambert, D. L. & Allende Prieto, C. The chemical compositions of Galactic disc F and G dwarfs. *Mon. Not. R. Astron. Soc.* **340**, 304–340 (2003).
30. Asplund, M., Grevesse, N., Sauval, A. J. & Scott, P. The chemical composition of the Sun. *Annu. Rev. Astron. Astrophys.* **47**, 481–522 (2009).
31. Morel, T. et al. Atmospheric parameters and chemical properties of red giants in the CoRoT asteroseismology fields. *Astron. Astrophys.* **564**, A119 (2014).
32. Bruntt, H. et al. Accurate fundamental parameters for 23 bright solar-type stars. *Mon. Not. R. Astron. Soc.* **405**, 1907–1923 (2010).
33. Morel, T. The chemical composition of α Centauri AB revisited. *Astron. Astrophys.* **615**, A172 (2018).
34. Bergemann, M., Lind, K., Collet, R., Magic, Z. & Asplund, M. Non-LTE line formation of Fe in late-type stars — I. Standard stars with 1D and 3D model atmospheres. *Mon. Not. R. Astron. Soc.* **427**, 27–49 (2012).
35. Bergemann, M. & Cescutti, G. Chromium: NLTE abundances in metal-poor stars and nucleosynthesis in the Galaxy. *Astron. Astrophys.* **522**, A9 (2010).
36. Bergemann, M., Pickering, J. C. & Gehren, T. NLTE analysis of Co I/Co II lines in spectra of cool stars with new laboratory hyperfine splitting constants. *Mon. Not. R. Astron. Soc.* **401**, 1334–1346 (2010).
37. Bergemann, M. et al. Red supergiant stars as cosmic abundance probes. II. NLTE effects in J-band silicon lines. *Astrophys. J.* **764**, 115 (2013).
38. Bergemann, M. et al. Non-local thermodynamic equilibrium stellar spectroscopy with 1D and 3D models. I. Methods and application to magnesium abundances in standard stars. *Astrophys. J.* **847**, 15 (2017).
39. Bergemann, M. & Gehren, T. NLTE abundances of Mn in a sample of metal-poor stars. *Astron. Astrophys.* **492**, 823–831 (2008).
40. Bergemann, M. et al. Observational constraints on the origin of the elements. I. 3D NLTE formation of Mn lines in late-type stars. *Astron. Astrophys.* **631**, A80 (2019).
41. Noyes, R. W., Hartmann, L. W., Baliunas, S. L., Duncan, D. K. & Vaughan, A. H. Rotation, convection, and magnetic activity in lower main-sequence stars. *Astrophys. J.* **279**, 763–777 (1984).
42. Henry, T. J., Soderblom, D. R., Donahue, R. A. & Baliunas, S. L. A survey of Ca II H and K chromospheric emission in southern solar-type stars. *Astron. J.* **111**, 439 (1996).
43. Wright, J. T. Do we know of any Maunder minimum stars? *Astron. J.* **128**, 1273 (2004).
44. Mamajek, E. E. & Hillenbrand, L. A. Improved age estimation for solar-type dwarfs using activity-rotation diagnostics. *Astrophys. J.* **687**, 1264–1293 (2008).
45. Zasowski, G. et al. Target selection for the apache point observatory Galactic evolution experiment (APOGEE). *Astron. J.* **146**, 81 (2013).
46. Zasowski, G. et al. Target selection for the SDSS-IV APOGEE-2 survey. *Astron. J.* **154**, 198 (2017).
47. Bovy, J. galpy: a Python library for galactic dynamics. *Astrophys. J. Suppl. Ser.* **216**, 29 (2015).
48. GravityCollaboration et al. Detection of the gravitational redshift in the orbit of the star S2 near the Galactic centre massive black hole. *Astron. Astrophys.* **615**, L15 (2018).
49. Bennett, M. & Bovy, J. Vertical waves in the solar neighbourhood in Gaia DR2. *Mon. Not. R. Astron. Soc.* **482**, 1417–1425 (2019).
50. Schönrich, R., Binney, J. & Dehnen, W. Local kinematics and the local standard of rest. *Mon. Not. R. Astron. Soc.* **403**, 1829–1833 (2010).
51. Jenkins, J. M. et al. The TESS science processing operations center. In *Software and Cyberinfrastructure for Astronomy IV* Vol. 9913 *Proc. SPIE* 99133E (2016).
52. Lund, M. N., Handberg, R., Kjeldsen, H., Chaplin, W. J. & Christensen-Dalsgaard, J. Data preparation for asteroseismology with TESS. In *European Physical Journal Web of Conferences* Vol. 160, 01005 (2017).
53. Kjeldsen, H. et al. Solar-like oscillations in α Centauri B. *Astrophys. J.* **635**, 1281–1290 (2005).
54. Bedding, T. R. et al. Solar-like oscillations in the G2 subgiant β hydri from dual-site observations. *Astrophys. J.* **663**, 1315–1324 (2007).
55. Benomar, O., Appourchaux, T. & Baudin, F. The solar-like oscillations of HD 49933: a Bayesian approach. *Astron. Astrophys.* **506**, 15–32 (2009).
56. Gaulme, P., Appourchaux, T. & Boumier, P. Mode width fitting with a simple Bayesian approach. Application to CoRoT targets HD 181420 and HD 49933. *Astron. Astrophys.* **506**, 7–14 (2009).
57. Mosser, B. et al. Spin down of the core rotation in red giants. *Astron. Astrophys.* **548**, A10 (2012).
58. Corsaro, E. & De Ridder, J. DIAMONDS: a new Bayesian nested sampling tool. Application to peak bagging of solar-like oscillations. *Astron. Astrophys.* **571**, A71 (2014).
59. Corsaro, E., De Ridder, J. & García, R. A. Bayesian peak bagging analysis of 19 low-mass low-luminosity red giants observed with Kepler. *Astron. Astrophys.* **579**, A83 (2015).
60. Vrard, M. et al. Helium signature in red giant oscillation patterns observed by Kepler. *Astron. Astrophys.* **579**, A84 (2015).
61. Nielsen, M. B., Schunker, H., Gizon, L., Schou, J. & Ball, W. H. Limits on radial differential rotation in Sun-like stars from parametric fits to oscillation power spectra. *Astron. Astrophys.* **603**, A6 (2017).
62. Roxburgh, I. W. Anomalies in the Kepler asteroseismic legacy project SATA. A re-analysis of 16 Cyg A and B, KIC 8379927 and 6 solar-like stars. *Astron. Astrophys.* **604**, A42 (2017).
63. García Saravia Ortiz de Montellano, A., Hekker, S. & Themeßl, N. Automated asteroseismic peak detections. *Mon. Not. R. Astron. Soc.* **476**, 1470–1496 (2018).
64. Benomar, O. et al. Asteroseismic detection of latitudinal differential rotation in 13 Sun-like stars. *Science* **361**, 1231–1234 (2018).
65. Kallinger, T., Beck, P. G., Stello, D. & Garcia, R. A. Non-linear seismic scaling relations. *Astron. Astrophys.* **616**, A104 (2018).
66. Davies, G. R. et al. Why should we correct reported pulsation frequencies for stellar line-of-sight Doppler velocity shifts? *Mon. Not. R. Astron. Soc.* **445**, L94–L98 (2014).
67. Casagrande, L. & VandenBerg, D. A. Synthetic stellar photometry — II. Testing the bolometric flux scale and tables of bolometric corrections for the Hipparcos/Tycho, Pan-STARRS1, SkyMapper, and JWST systems. *Mon. Not. R. Astron. Soc.* **475**, 5023–5040 (2018).

68. Stassun, K. G. & Torres, G. Eclipsing binaries as benchmarks for trigonometric parallaxes in the Gaia era. *Astron. J.* **152**, 180 (2016).
69. Torres, G. et al. Improved spectroscopic parameters for transiting planet hosts. *Astrophys. J.* **757**, 161 (2012).
70. Salaris, M., Chieffi, A. & Straniero, O. The alpha-enhanced isochrones and their impact on the FITS to the Galactic globular cluster system. *Astrophys. J.* **414**, 580–600 (1993).
71. Rendle, B. M. et al. AIMS — a new tool for stellar parameter determinations using asteroseismic constraints. *Mon. Not. R. Astron. Soc.* **484**, 771–786 (2019).
72. Ong, J. M. J. & Basu, S. Explaining deviations from the scaling relationship of the large frequency separation. *Astrophys. J.* **870**, 41 (2019).
73. SilvaAguirre, V. et al. Standing on the shoulders of dwarfs: the Kepler asteroseismic LEGACY sample. II. Radii, masses, and ages. *Astrophys. J.* **835**, 173 (2017).
74. Mosumgaard, J. R., Ball, W. H., SilvaAguirre, V., Weiss, A. & Christensen-Dalsgaard, J. Stellar models with calibrated convection and temperature stratification from 3D hydrodynamics simulations. *Mon. Not. R. Astron. Soc.* **478**, 5650–5659 (2018).
75. Ball, W. H. & Gizon, L. Surface-effect corrections for oscillation frequencies of evolved stars. *Astron. Astrophys.* **600**, A128 (2017).
76. Lebreton, Y. & Goupil, M. J. Asteroseismology for 'à la carte' stellar age-dating and weighing. Age and mass of the CoRoT exoplanet host HD 52265. *Astron. Astrophys.* **569**, A21 (2014).
77. Yildiz, M., Çelik Orhan, Z. & Kayhan, C. Fundamental properties of Kepler and CoRoT targets. III. Tuning scaling relations using the first adiabatic exponent. *Mon. Not. R. Astron. Soc.* **462**, 1577–1590 (2016).
78. Lacey, C. & Cole, S. Merger rates in hierarchical models of galaxy formation. *Mon. Not. R. Astron. Soc.* **262**, 627–649 (1993).
79. Belokurov, V., Erkal, D., Evans, N. W., Koposov, S. E. & Deason, A. J. Co-formation of the disc and the stellar halo. *Mon. Not. R. Astron. Soc.* **478**, 611–619 (2018).
80. Mo, H., van den Bosch, F. C. & White, S. *Galaxy Formation and Evolution* (Cambridge University Press, 2010).
81. Myeong, G. C., Vasiliev, E., Iorio, G., Evans, N. W. & Belokurov, V. Evidence for two early accretion events that built the Milky Way stellar halo. *Mon. Not. R. Astron. Soc.* **488**, 1235–1247 (2019).
82. Correa, C. A., Wyithe, J. S. B., Schaye, J. & Duffy, A. R. The accretion history of dark matter haloes. I. The physical origin of the universal function. *Mon. Not. R. Astron. Soc.* **450**, 1514–1520 (2015).
83. Correa, C. A., Wyithe, J. S. B., Schaye, J. & Duffy, A. R. The accretion history of dark matter haloes. II. The connections with the mass power spectrum and the density profile. *Mon. Not. R. Astron. Soc.* **450**, 1521–1537 (2015).
84. Correa, C. A., Wyithe, J. S. B., Schaye, J. & Duffy, A. R. The accretion history of dark matter haloes. III. A physical model for the concentration-mass relation. *Mon. Not. R. Astron. Soc.* **452**, 1217–1232 (2015).

Acknowledgements

This paper includes data collected by the TESS mission, which are publicly available from the Mikulski Archive for Space Telescopes (MAST). Resources supporting this work were provided by the NASA High-End Computing (HEC) Program through the NASA Advanced Supercomputing (NAS) Division at Ames Research Center for the production of the SPOC data products. W.J.C. acknowledges support from the UK Science and Technology Facilities Council (STFC) and UK Space Agency. Funding for the Stellar Astrophysics Centre is provided by The Danish National Research Foundation (grant agreement number DNRF106). This research was partially conducted during the Exostar19 programme at the Kavli Institute for Theoretical Physics at UC Santa Barbara, which was supported in part by the National Science Foundation under grant number NSF PHY-1748958. A.M., J.T.M., F.V. and J.M. acknowledge support from the ERC Consolidator Grant funding scheme (project ASTEROCHRONOMETRY, grant agreement number 772293). F.V. acknowledges the support of a Fellowship from the Center for Cosmology and AstroParticle Physics at The Ohio State University. W.H.B. and M.B.N. acknowledge support from the UK Space Agency. K.J.B. is supported by the National Science Foundation under award AST-1903828. M.B.N. acknowledges partial support from the NYU Abu Dhabi Center for Space Science under grant number G1502. A.M.S. is partially supported by the Spanish Government (ESP2017-82674-R) and Generalitat de Catalunya (2017-SGR-1131). T.M. acknowledges financial support from Belspo for contract PRODEX PLATO. H.K. acknowledges support from the European Social Fund via the Lithuanian Science Council grant number 09.3.3-LMT-K-712-01-0103. S.B. acknowledges support from NSF grant AST-1514676 and NASA grant 80NSSC19K0374. V.S.A. acknowledges support from the Independent Research Fund Denmark (research grant 7027-00096B). D.H. acknowledges support by the National Aeronautics and Space Administration (80NSSC18K1585, 80NSSC19K0379) awarded through the TESS Guest Investigator Program and by the National Science Foundation (AST-1717000). T.S.M. acknowledges support from a visiting fellowship at the Max Planck Institute for Solar System Research. Computational resources were provided through XSEDE allocation TG-AST090107. D.L.B. acknowledges support from NASA under grant NNX16AB76G. T.L.C. acknowledges support from the European Union's Horizon 2020 research and innovation programme under the Marie Skłodowska-Curie grant agreement number 792848 (PULSATION). This work was supported by FCT/MCTES through national funds (PIDDAC) by means of grant UID/FIS/04434/2019. K.J.B., S.H., J.S.K. and N.T. are supported by the European Research Council under the European Community's Seventh Framework Programme (FP7/2007-2013)/ERC grant agreement number 338251 (StellarAges). E.C. is funded by the European Union's Horizon 2020 research and innovation program under the Marie Sklodowska-Curie grant agreement number 664931. L.G.-C. acknowledges support from the MINECO FPI-SO doctoral research project SEV-2015-0548-17-2 and predoctoral contract BES-2017-082610. P.G. is supported by the German space agency (Deutsches Zentrum für Luft- und Raumfahrt) under PLATO data grant 50OO1501. R.K. acknowledges support from the UK Science and Technology Facilities Council (STFC), under consolidated grant ST/L000733/1. M.S.L. is supported by the Carlsberg Foundation (grant agreement number CF17-076). Z.C.O., S.O. and M.Y. acknowledge support from the Scientific and Technological Research Council of Turkey (TÜBİTAK:118F352). S.M. acknowledges support from the Spanish ministry through the Ramon y Cajal fellowship number RYC-2015-17697. T.S.R. acknowledges financial support from Premiale 2015 MITiC (PI B. Garilli). R.Sz. acknowledges the support from NKFIH grant project No. K-115709, and the Lendület program of the Hungarian Academy of Science (project number 2018-7/2019). J.T. acknowledges support was provided by NASA through the NASA Hubble Fellowship grant number 51424 awarded by the Space Telescope Science Institute, which is operated by the Association of Universities for Research in Astronomy, Inc., for NASA, under contract NAS5-26555. This work was supported by FEDER through COMPETE2020 (POCI-01-0145-FEDER-030389. A.M.B. acknowledges funding from the European Union's Horizon 2020 research and innovation program under the Marie Sklodowska-Curie grant agreement No 749962 (project THOT). A.M. and P.R. acknowledge the support of the Government of India, Department of Atomic Energy, under Project No. 12-R&D-TFR-6.04-0600. K.J.B. is an NSF Astronomy and Astrophysics Postdoctoral Fellow and DIRAC Fellow.

Author contributions

W.J.C. led the project, with help from A.M.S., A.M., S.B. and W.H.B. W.J.C., H.K., W.H.B., H.M.A., T.R.B., R.A.G., D.H., K.J.B., D.L.B., O.B., L.B., T.L.C., E.C., L.G.-C., G.R.D., Y.P.E., P.G., H.G., O.J.H., A.H., S.H., R.H., A.J., R.K., J.S.K., T.K., M.S.L., S.M., B.M., A.M.B., M.B.N., I.W.R., H.S., R.S., N.T., A.E.L.T., M.V. and T.M.W. worked on extracting mode parameters from the TESS data. R.H. and M.N.L. oversaw production of the TESS lightcurves for the asteroseismic analysis. A.M.S., A.M., S.B., W.H.B., A.S., K.V., J.R.M., V.S.A., A.M., P.R., Y.B., J.O., P.B., M.B., K.J.B., D.B., Z.C.O., M.P.D.M., Z.G., S.H., J.M., S.O., B.M.R., T.S.R., D.S., J.T., W.E.v.R., A.W. and M.Y. worked on modelling ν Indi. T.M. performed the spectroscopic analysis of the archival HARPS and FEROS data on ν Indi. M.B. assessed the impact of NLTE on the spectroscopic analysis. R.E. performed the chromospheric activity analysis of ν Indi. J.T.M. performed the kinematics analysis and comparison of the chemistry of ν Indi with samples of Milky Way stars, and F.V. computed the theoretical prior based on hierarchical cosmological models of structure formation. D.H., K.G.S. and B.S. provided estimates of the luminosity of ν Indi. J.C.-D., H.K., W.J.C., T.R.B., S.D.K. and S.B. are key architects of TASC (members of its board), while G.R.R., J.M.J., D.W.L., R.K.V. and J.N.W. are key architects of the TESS Mission. W.J.C., D.H., T.A., A.M.S., O.C., R.A.G. and T.S.M. oversaw the TASC working groups on solar-like oscillators and, with M.S. and T.L.C., oversaw the selection of short-cadence targets for asteroseismic studies of solar-like oscillators with TESS, which included ensuring ν Indi was included on the list (and hence received the TESS short-cadence data needed to make this study possible). All authors have contributed to the interpretation of the data and the results, and to discussion and comments on the paper.

Competing interests

The authors declare no competing interests.

Additional information

Extended data is available for this paper at https://doi.org/10.1038/s41550-019-0975-9.

Correspondence and requests for materials should be addressed to W.J.C.

Reprints and permissions information is available at www.nature.com/reprints.

Publisher's note Springer Nature remains neutral with regard to jurisdictional claims in published maps and institutional affiliations.

[1]School of Physics and Astronomy, University of Birmingham, Birmingham, UK. [2]Stellar Astrophysics Centre (SAC), Department of Physics and Astronomy, Aarhus University, Aarhus, Denmark. [3]Kavli Institute for Theoretical Physics, University of California, Santa Barbara, CA, USA. [4]Institute of Space Sciences (ICE, CSIC), Barcelona, Spain. [5]Institut d'Estudis Espacials de Catalunya, Barcelona, Spain. [6]Space Sciences, Technologies and Astrophysics Research (STAR) Institute, Université de Liège, Liège, Belgium. [7]Center for Cosmology and AstroParticle Physics, The Ohio State University, Columbus, OH, USA. [8]Department of Physics, The Ohio State University, Columbus, OH, USA. [9]Institute of Theoretical Physics and Astronomy, Vilnius University, Vilnius, Lithuania. [10]Department of Astronomy, Yale University, New Haven, CT, USA. [11]Homi Bhabha Centre for Science Education, TIFR, Mumbai, India. [12]Tata Institute of Fundamental Research, Mumbai, India. [13]LESIA, Observatoire de Paris, Université PSL, CNRS, Sorbonne Université, Université de Paris, Meudon, France. [14]Université Rennes, CNRS, Institut de Physique de Rennes, UMR, Rennes, France. [15]Université Paris-Sud, Institut d'Astrophysique Spatiale, Orsay, France. [16]Sydney Institute for Astronomy, School of Physics, University of Sydney, Sydney, New South Wales, Australia. [17]Université Côte d'Azur, Observatoire de la Côte d'Azur, CNRS, Laboratoire Lagrange, Nice, France. [18]IRFU, CEA, Université Paris-Saclay, Gif-sur-Yvette, France. [19]AIM, CEA, CNRS, Université Paris-Saclay, Université Paris Diderot, Sorbonne Paris Cité, Gif-sur-Yvette, France. [20]Institute for Astronomy, University of Hawai'i, Honolulu, HI, USA. [21]Department of Physics and Astronomy, Iowa State University, Ames, IA, USA. [22]Space Science Institute, Boulder, CO, USA. [23]Max-Planck-Institut für Sonnensystemforschung, Göttingen, Germany. [24]Department of Physics and Astronomy, Vanderbilt University, Nashville, TN, USA. [25]Vanderbilt Initiative in Data-intensive Astrophysics, Nashville, TN, USA. [26]Division of Sciences, New York University Abu Dhabi, Abu Dhabi, United Arab Emirates. [27]Center for Space Science, NYUAD Institute, New York University Abu Dhabi, Abu Dhabi, United Arab Emirates. [28]Department for Geophysics, Meteorology and Astrophysics, Institute of Physics, Karl-Franzens University of Graz, NAWI Graz, Austria. [29]Instituto de Astrofísica de Canarias, La Laguna, Tenerife, Spain. [30]Departamento de Astrofisica, Universidad de La Laguna, La Laguna, Tenerife, Spain. [31]DIRAC Institute, Department of Astronomy, University of Washington, Seattle, WA, USA. [32]Max Planck Institute for Astronomy, Heidelberg, Germany. [33]Dept. of Chemistry and Physics, Florida Gulf Coast University, Fort Myers, FL, USA. [34]Solar Science Observatory, NAOJ and Department of Astronomical Science, Sokendai (GUAS), Mitaka, Tokyo, Japan. [35]Instituto de Astrofísica e Ciências do Espaço, Universidade do Porto, CAUP, Porto, Portugal. [36]Departamento de Física e Astronomia, Faculdade de Ciências da Universidade do Porto, Porto, Portugal. [37]Department of Astronomy and Space Sciences, Ege University, İzmir, Turkey. [38]INAF, Osservatorio Astrofisico di Catania, Catania, Italy. [39]INAF-IAPS, Istituto di Astrofisica e Planetologia Spaziali, Roma, Italy. [40]High Altitude Observatory, National Center for Atmospheric Research, Boulder, CO, USA. [41]Department of Astronomy, New Mexico State University, Las Cruces, NM, USA. [42]Department of Physics, Institute for Advanced Studies in Basic Sciences, Zanjan, Iran. [43]Center for Exoplanets and Habitable Worlds, The Pennsylvania State University, University Park, PA, USA. [44]Department of Astronomy and Astrophysics, The Pennsylvania State University, University Park, PA, USA. [45]Department of Physics, University of Zanjan, Zanjan, Iran. [46]NASA Ames Research Center, Moffett Field, CA, USA. [47]Centre for Fusion, Space, and Astrophysics, Department of Physics, University of Warwick, Coventry, UK. [48]Institute of Astronomy, University of Vienna, Vienna, Austria. [49]Center for Astrophysics, Harvard and Smithsonian, Cambridge, MA, USA. [50]Department of Physics, Kavli Institute for Astrophysics and Space Research, Massachusetts Institute of Technology, Cambridge, MA, USA. [51]Osservatorio Astronomico di Padova, INAF, Padua, Italy. [52]Astronomy Unit, Queen Mary University of London, London, UK. [53]Department of Earth, Atmospheric and Planetary Sciences, Massachusetts Institute of Technology, Cambridge, MA, USA. [54]Department of Aeronautics and Astronautics, MIT, Cambridge, MA, USA. [55]Astrophysics Group, Lennard-Jones Laboratories, Keele University, Keele, UK. [56]School of Physics, The University of New South Wales, Sydney, New South Wales, Australia. [57]Konkoly Observatory, CSFK, Budapest, Hungary. [58]MTA CSFK Lendület Near-Field Cosmology Research Group, Budapest, Hungary. [59]Hubble Fellow, Institute for Astronomy, University of Hawai'i, Honolulu, HI, USA. [60]Max-Planck-Institut für Astrophysik, Garching, Germany. [61]Research School of Astronomy and Astrophysics, Mount Stromlo Observatory, The Australian National University, Canberra, Australian Capital Territory, Australia. [62]Department of Astrophysical Sciences, Princeton University, Princeton, NJ, USA.
*e-mail: w.j.chaplin@bham.ac.uk

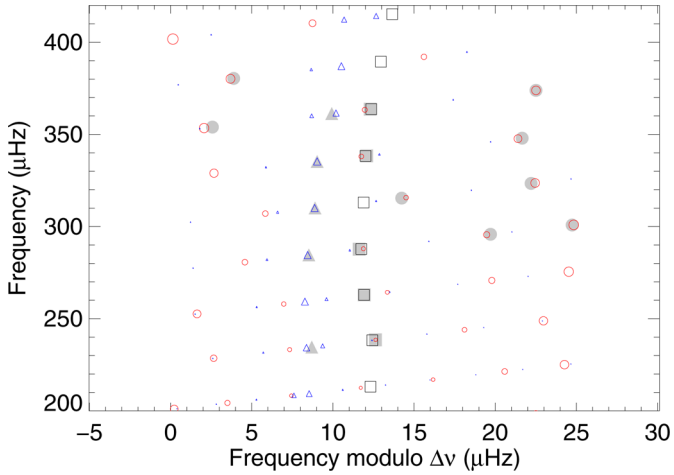

Extended Data Fig. 1 | An échelle diagram showing the observed frequencies (in grey) and the best-fitting model frequencies (coloured symbols). The diagram was made by dividing the spectrum into segments of length equal to the average frequency separation $\Delta\nu$ between consecutive overtones, which were then stacked in ascending order, so one plots ν versus (ν mod $\Delta\nu$). The $l = 0$ (radial) modes are plotted with square symbols, the $l = 1$ (dipole) modes are plotted with circular symbols, and the $l = 2$ (quadrupole) modes are plotted with triangular symbols. Symbol sizes reflect the relative visibilities of the different modes, with a suitable correction included to reflect the impact of mixing on the mode inertia. All model frequencies are plotted, irrespective of whether we were able to report a reliable observed frequency for them.

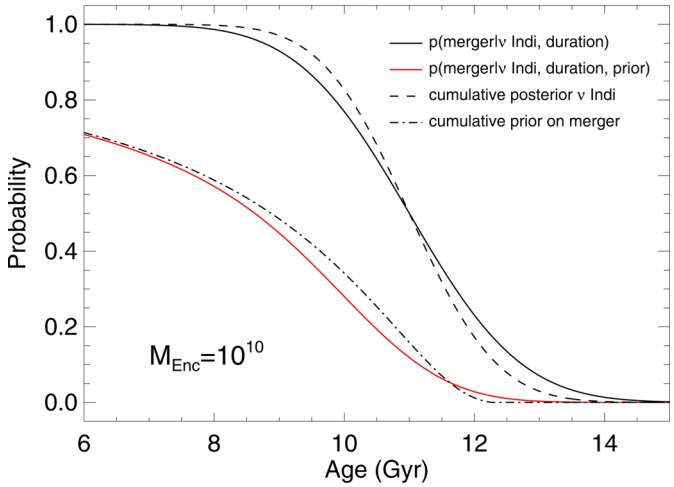

Extended Data Fig. 2 | Inference on the epoch of the Gaia–Enceladus merger. The dashed black line shows the measured cumulative posterior on ν Indi. The dot-dashed black line is the estimated cumulative prior probability for the merger assuming a virial mass of the Gaia–Enceladus dark-matter halo of $M_{\rm Enc} = 1 \times 10^{10}$ $M_\odot$. The solid black line shows the cumulative probability for the merger, dependent on the estimated age of ν Indi and the assumed 2-Gyr-wide merger duration; while the solid red line shows the cumulative probability for the merger also taking into account the merger prior (different in each panel, since this depends on $M_{\rm Enc}$).

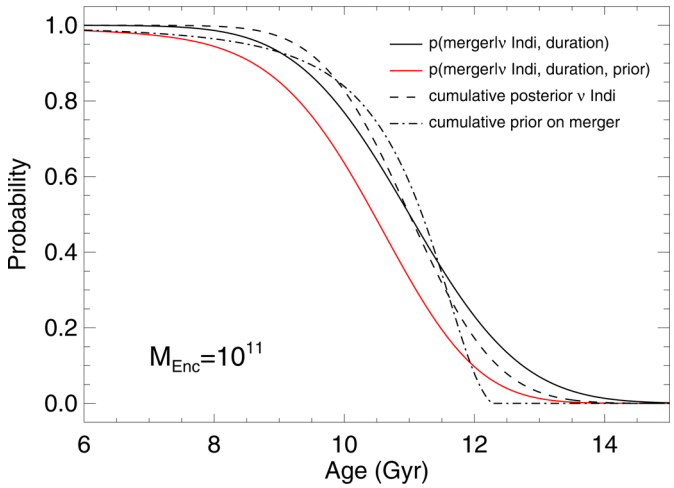

Extended Data Fig. 3 | As for Extended Data Fig. 2, but now assuming a virial mass of the Gaia–Enceladus dark-matter halo of 1×10^{11} $M_{\odot}$. We note the measured cumulative posterior on ν Indi (dashed black line) and the cumulative probability for the merger (dependent on the estimated age of ν Indi and the assumed 2-Gyr-wide merger duration; black line) are the same as in Extended Data Fig. 2.